
**Separation Science and Technology**
Publication details, including instructions for authors and subscription information:
http://www.informaworld.com/smpp/title~content=t713708471

# Treatment of Aqueous Effluents Containing Phenol by the $O_3$, $O_3$-UV, and $O_3$-$H_2O_2$ Processes: Experimental Study and Neural Network Modeling

L. L. C. Catorceno[a]; K. R. B. Nogueira[a]; A. C. S. C. Teixeira[a]
[a] Chemical Engineering Department, University of São Paulo, Brazil

Online publication date: 19 July 2010

**To cite this Article** Catorceno, L. L. C. , Nogueira, K. R. B. and Teixeira, A. C. S. C.(2010) 'Treatment of Aqueous Effluents Containing Phenol by the $O_3$, $O_3$-UV, and $O_3$-$H_2O_2$ Processes: Experimental Study and Neural Network Modeling', Separation Science and Technology, 45: 11, 1521 — 1528
**To link to this Article: DOI:** 10.1080/01496395.2010.487453
**URL:** http://dx.doi.org/10.1080/01496395.2010.487453

*Separation Science and Technology*, 45: 1521–1528, 2010

ISSN: 0149-6395 print/1520-5754 online
DOI: 10.1080/01496395.2010.487453

Taylor & Francis
Taylor & Francis Group

# Treatment of Aqueous Effluents Containing Phenol by the $O_3$, $O_3$-UV, and $O_3$-$H_2O_2$ Processes: Experimental Study and Neural Network Modeling

**L. L. C. Catorceno, K. R. B. Nogueira, and A. C. S. C. Teixeira**
*Chemical Engineering Department, University of São Paulo, Brazil*

**In this work, the oxidation of the model pollutant phenol has been studied by means of the $O_3$, $O_3$-UV, and $O_3$-$H_2O_2$ processes. Experiments were carried out in a fed-batch system to investigate the effects of initial dissolved organic carbon concentration, initial, ozone concentration in the gas phase, the presence or absence of UVC radiation, and initial hydrogen peroxide concentration. Experimental results were used in the modeling of the degradation processes by neural networks in order to simulate DOC-time profiles and evaluate the relative importance of process variables.**

**Keywords** advanced oxidation processes; hydrogen peroxide; neural networks; ozone; phenol



## INTRODUCTION

The problem of scarce quality fresh water is worsened by the contamination of water resources by toxic or recalcitrant substances. Conventional wastewater treatment technologies usually transfer chemical pollutants from one phase to another, and in many situations biological activated-sludge systems are not suitable. In this context, ozone-based Advanced Oxidation Processes (AOPs) have proved to be effective for the degradation of hazardous compounds like phenol and derivatives present in wastewaters from several industrial processes (coke plants, petroleum refinery, pulp and paper, polymers, textiles, soaps and detergents, pesticides, etc.). The literature presents investigations concerning such applications (1–8).

The ozone molecule can undergo direct reactions with many other chemical species, such as oxidation, cycloaddition, and electrophilic substitution reactions (8). Concerning the first, suffice it to say only that ozone has a high standard reduction potential ($E^o = 2.07$ V). The other types of reactions describe the ozonation of compounds such as phenol and derivatives (8). According to the literature (8,9) the strong electron donor behavior of the $-OH$ group stabilizes the carbocation formed, so that the fast ozonation of phenol occurs mainly at *ortho* and *para* positions of the hydroxyl group. Direct oxidation by ozone is a selective reaction with rate constants in the range $k = 1$–$10^3\ L\,mol^{-1}\,s^{-1}$, and generally dominates under acidic conditions (pH < 4) (9).

Indirect reactions of ozone involve oxidants such as hydroxyl radicals ($^{\bullet}OH$), known to be very reactive species ($E^o = 2.80$ V) formed from the decomposition of ozone or from other direct ozone reactions (8), which react with the majority of organic pollutants with low selectivity (rate constants in the range $k = 10^8$–$10^{10}\ L\,mol^{-1}\,s^{-1}$) (10). According to Beltrán (8), the mechanism of Staehelin, Hoigné, and Bühler (SHB) is generally accepted for the decomposition of ozone in water, although at high pH values the mechanism of Tomiyasu, Fukutomi, and Gordon (TFG) is considered most representative. Sets of initiation, propagation, and termination reactions for the SHB and TFG mechanisms are presented by the author (8), who points out that the reactions of ozone with hydroxyl ($OH^-$) and hydroperoxide ($HO_2^-$) ions are responsible for the initiation steps. Superoxide radical anions ($O_2^{\bullet -}$), generated by the reaction with $OH^-$ ions and from the decomposition of $HO_2^{\bullet}$ radicals, are involved in propagation steps. Their rapid reaction with $O_3$ yields free radicals, such as the ozonide ion radical ($O_3^{\bullet -}$) that leads to $^{\bullet}OH$ radicals (8).

In addition to these routes, the direct photolysis of aqueous $O_3$ under UVC radiation generates $H_2O_2$ which undergoes further photolysis and/or reacts with $O_3$ yielding $^{\bullet}OH$ radicals (9). Finally, hydrogen peroxide is frequently combined in the $O_3$-$H_2O_2$ AOP that proceeds in aqueous systems through an extensively studied mechanism (8).

In this work, the $O_3$, $O_3$-UV, and $O_3$-$H_2O_2$ processes were investigated concerning the effects of operational variables upon the removal of dissolved organic carbon (DOC) concentration. The results were used in the modeling of the degradation processes by neural networks.

Received 7 December 2009; accepted 12 February 2010.
Address correspondence to A. C. S. C. Teixeira, Chemical Engineering Department, University of São Paulo, Av. Prof. Luciano Gualberto, travessa 3, 380, CEP 05508-900, São Paulo, SP, Brazil. Tel.: +55-1130912263; Fax: +55-1138132380. E-mail: acscteix@usp.br

## EXPERIMENTAL

Phenol (Sigma-Aldrich, 99%) and hydrogen peroxide (Merck, 30% w/w $H_2O_2$ in water) were used. Solutions were prepared with distilled water.

A schematic view of the experimental apparatus is shown in Fig. 1. The experiments were carried out in a 3.8 L jacketed annular glass reactor, equipped with a centrifugal pump to provide liquid circulation at 1.5 L min$^{-1}$. A low pressure mercury vapor lamp (Osram HNS OFR, 11 W), placed inside a quartz-well immersed within the reactor, was used as the light source. Figure 2 shows the spectra of the power distribution of the light source (with the main emission line centered at 253.7 nm) and the transmittance of the quartz well. The temperature of the liquid was controlled at $20 \pm 1$°C by means of a thermo-regulated bath (Julabo, model ME F25). The pH of the aqueous solution was initially adjusted by dripping an aqueous solution of $H_2SO_4$ (Merck, 95–97%); in the experiments with $O_3$ and $O_3$-UV processes, pH was allowed to change with time, whereas in $O_3$-$H_2O_2$ experiments it was kept constant ($\pm$0.05) at the initial value, as discussed later. The reactor was operated in the fed-batch mode with an oxygen stream containing $O_3$ bubbled in the liquid through a sinterized glass plate, delivered by an electrical discharge ozone generator (Multivacuo, model MV-06/220). The gas flow rate was controlled at 1 L min$^{-1}$ by a regulating valve and a mass flow meter (Matheson, model 8170). Ozone in the incoming gas was monitored at 253.7 nm using a Shimadzu spectrophotometer (model MultiSpec 1501) equipped with a quartz flow cell. Non-reacted ozone leaving the reactor was decomposed in an aqueous solution containing 1% KI (Sigma-Aldrich, 99%) and adsorbed on activated carbon.

The experimental procedure involved the following steps. The aqueous solution containing phenol was fed to the reactor, the centrifugal pump and the thermo-regulated bath were started, and the pH was adjusted by adding $H_2SO_4$ solution. After ozone concentration in the gas phase attained the desired steady value, the $O_2 + O_3$ gas stream was allowed to flow through the solution inside the reactor at time $t = 0$. The lamp was immediately switched on

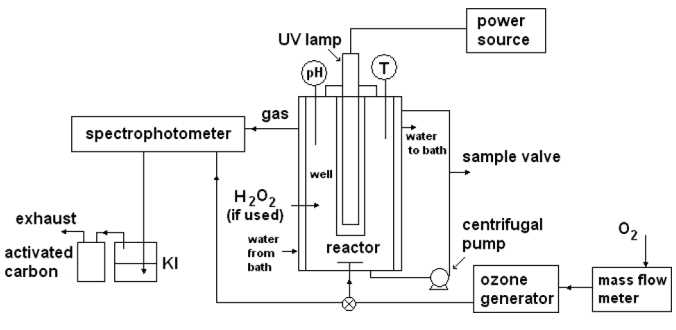


FIG. 1. Schematic view of the experimental apparatus.

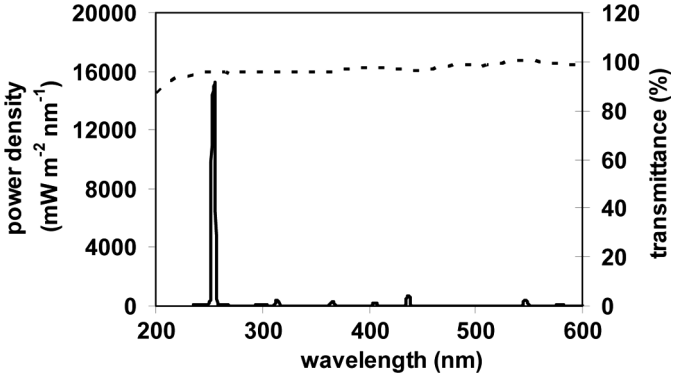


FIG. 2. Spectral distribution of the low pressure mercury lamp emission power (solid line), and transmittance of the quartz well (dotted line).

($O_3$-UV process) or the $H_2O_2$ solution was injected in the reactor ($O_3$-$H_2O_2$ process). Ten-milliliter liquid samples were then collected at specified times, and analyzed using a Shimadzu TOC-5000A equipment in order to quantify DOC concentration.

Fractional factorial experimental designs at two levels with additional experiments were carried out aiming to investigate the effects of the following variables: initial dissolved organic carbon concentration, $DOC_0$ (100 and 500 mg C L$^{-1}$); initial pH (3 and 11, $O_3$ and $O_3$-UV processes; 4 and 8, $O_3$-$H_2O_2$ process); ozone concentration in the gas phase, [$O_3$] (10 and 50 mg $O_3$ L$^{-1}$); UVC radiation (present or absent) or initial $H_2O_2$ concentration, $[H_2O_2]_0$ (0.1 and 10 mmol L$^{-1}$). The values in brackets refer to the minimum ($-1$) and maximum ($+1$) levels of the studied variables.

## RESULTS AND DISCUSSION

### Experimental Results

Preliminary experiments showed that DOC removal by the oxygen gas stream or by UV photolysis was less than 2% and 1.5% after 120 minutes, respectively, and could therefore be neglected. Tables 1 and 2 show the response variables and the conditions at which the experiments were run, in terms of the coded values of the independent variables. The corresponding DOC-time evolutions are shown in Figs. 3 to 5. For the low $DOC_0$ level ($102.9 \pm 13.3$ mg C L$^{-1}$), maximum DOC removals of 58.2% ($O_3$), 99.2% ($O_3$-UV), and 85.6% ($O_3$-$H_2O_2$) were obtained after 120 minutes; for the high level ($DOC_0 = 501.6 \pm 24.7$ mg C L$^{-1}$), however, the maximum removals of only 15.9%, 15%, and 29.8% were slowly achieved, respectively. The maximum removal rates of 0.63 mg C L$^{-1}$ min$^{-1}$ and 0.83 mg C L$^{-1}$ min$^{-1}$ were obtained for experiments P4 ($O_3$ process) and P7A ($O_3$-UV process), respectively. In the $O_3$-$H_2O_2$ system, a maximum removal rate of 2.28 mg C L$^{-1}$ min$^{-1}$ was obtained for high $[H_2O_2]_0$ and $pH_0$ 8 (experiment H7A).

TABLE 1
Experimental design in terms of coded independent variables and values of the responses for the $O_3$ and $O_3$-UV processes

| Experiment | $DOC_0$ | $[O_3]$ | $pH_0$ | UVC radiation | $DOC_0$ ($mg\,C\,L^{-1}$) | DOC removal (%) | DOC removal rate ($mg\,C\,L^{-1}\,min^{-1}$) |
|---|---|---|---|---|---|---|---|
| P1 | −1 | −1 | −1 | −1 | 103.5 | 34.4 | 0.29 |
| P1A | −1 | −1 | −1 | +1 | 99.7 | 44.4 | 0.35 |
| P2 | +1 | −1 | −1 | +1 | 505.9 | 6.4 | 0.26 |
| P3 | −1 | +1 | −1 | +1 | 94.9 | 94.0 | 0.75 |
| P3A | −1 | +1 | −1 | −1 | 97.5 | 58.2 | 0.53 |
| P4 | +1 | +1 | −1 | −1 | 503.0 | 15.9 | 0.63 |
| P5 | −1 | −1 | +1 | +1 | 97.2 | 46.5 | 0.38 |
| P5A | −1 | −1 | +1 | −1 | 104.5 | 33.7 | 0.32 |
| P6 | +1 | −1 | +1 | −1 | 502.9 | 8.7 | 0.38 |
| P7 | −1 | +1 | +1 | −1 | 107.4 | 50.2 | 0.52 |
| P7A | −1 | +1 | +1 | +1 | 92.9 | 99.2 | 0.83 |
| P8 | +1 | +1 | +1 | +1 | 485.8 | 15.0 | 0.77 |
| P9 | 0 | 0 | 0 | +1 | 281.0 | 33.1 | 0.79 |
| P10 | 0 | 0 | 0 | −1 | 273.6 | 21.9 | 0.48 |
| PC1 | −1 | 0 | 0 | −1 | 125.8 | 49.4 | 0.59 |
| PC2 | −1 | 0 | 0 | −1 | 124.2 | 51.1 | 0.59 |
| LPC1 | −1 | 0 | 0 | +1 | 85.3 | 93.7 | 0.69 |
| LPC2 | −1 | 0 | 0 | +1 | 86.0 | 90.5 | 0.71 |



Figures 3 to 5 show that most of the $DOC/DOC_0$-time curves cannot be described exclusively by simple zero- or first-order kinetic models. In fact, for the $O_3$, $O_3$-UV, and $O_3$-$H_2O_2$ processes these curves exhibit an initial induction period (up to about 15–20 minutes), characterized by a slow DOC removal which can be explained by the formation of oxidation intermediates. After this period, first-order kinetics seems to describe most of the experimental data. Furthermore, the curves suggest that recalcitrant intermediates were formed in some cases, since the

TABLE 2
Experimental design in terms of coded independent variables and values of the responses for the $O_3$-$H_2O_2$ process

| Experiment | $DOC_0$ | $[O_3]$ | $pH_0$ | $[H_2O_2]_0$ | $DOC_0$ ($mg\,C\,L^{-1}$) | DOC removal (%) | DOC removal rate ($mg\,C\,L^{-1}\,min^{-1}$) |
|---|---|---|---|---|---|---|---|
| H1 | −1 | −1 | −1 | −1 | 102.3 | 36.9 | 0.36 |
| H1A | −1 | −1 | −1 | +1 | 109.4 | 43.6 | 0.48 |
| H2 | +1 | −1 | −1 | +1 | 492.5 | 11.4 | 0.44 |
| H3 | −1 | +1 | −1 | +1 | 89.2 | 85.6 | 1.83 |
| H3A | −1 | +1 | −1 | −1 | 103.2 | 55.5 | 0.69 |
| H4 | +1 | +1 | −1 | −1 | 466.1 | 24.7 | 0.90 |
| H5 | −1 | −1 | +1 | +1 | 118.6 | 60.2 | 0.59 |
| H5A | −1 | −1 | +1 | −1 | 128.0 | 50.4 | 0.56 |
| H6 | +1 | −1 | +1 | −1 | 553.2 | 19.8 | 1.21 |
| H7 | −1 | +1 | +1 | −1 | 102.7 | 60.5 | 1.28 |
| H7A | −1 | +1 | +1 | +1 | 118.5 | 83.0 | 2.28 |
| H8 | +1 | +1 | +1 | +1 | 503.6 | 29.8 | 1.36 |
| H9 | 0 | 0 | 0 | −0.8 | 339.2 | 37.0 | 1.22 |
| H10 | 0 | 0 | 0 | 0 | 261.7 | 58.8 | 1.39 |
| HPC1 | −1 | 0 | 0 | 0 | 87.0 | 83.4 | 0.92 |
| HPC2 | −1 | 0 | 0 | 0 | 85.7 | 81.4 | 1.00 |

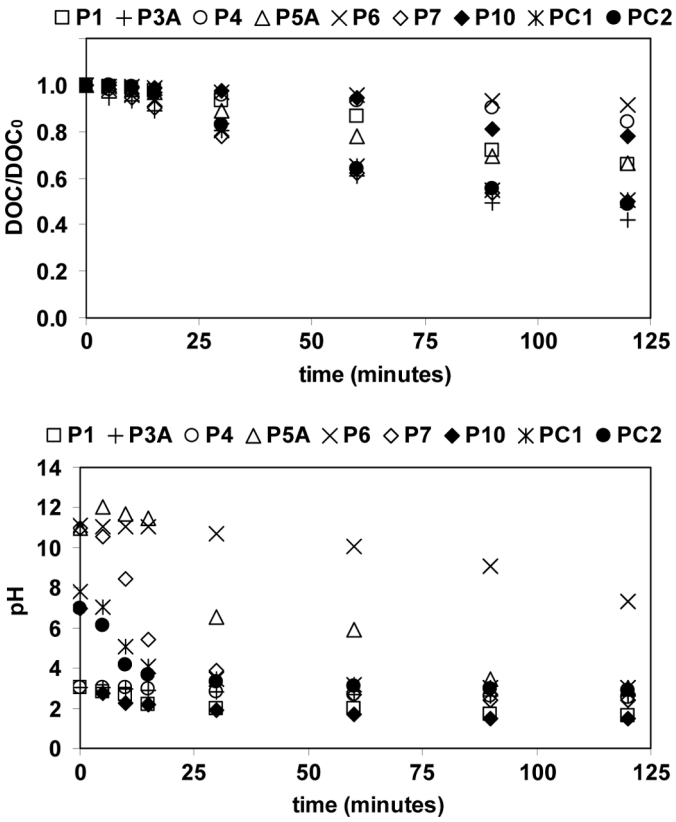


FIG. 3. Time variation of $DOC/DOC_0$ and pH for the $O_3$ process.

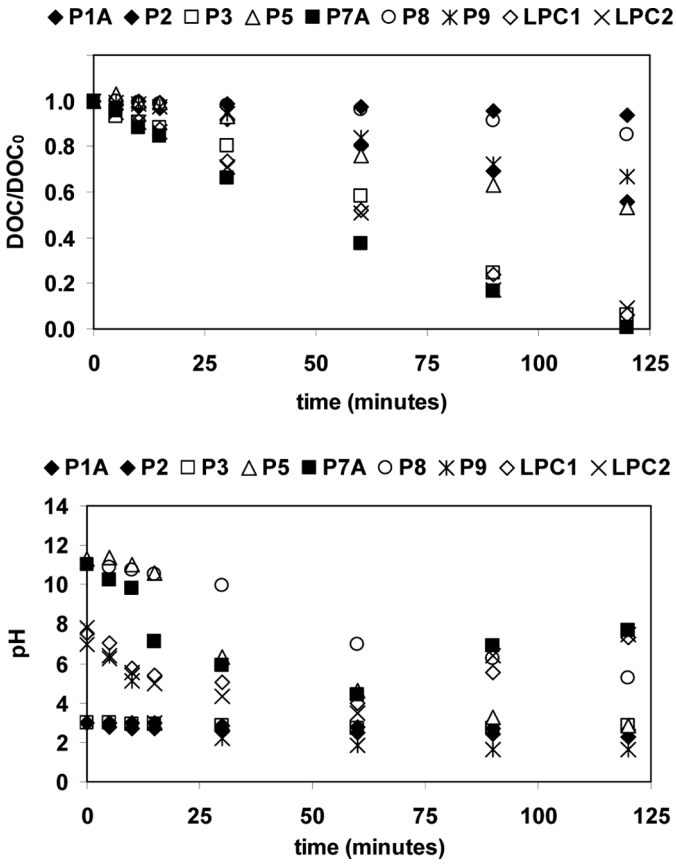


FIG. 4. Time variation of $DOC/DOC_0$ and pH for the $O_3$-UV process.

$DOC/DOC_0$ values stabilize after the period of a larger decrease rate.

For the lowest $DOC_0$ and in the absence of $H_2O_2$, the increase in ozone concentration from 10 to 50 mg $L^{-1}$ and UVC irradiation showed positive effects upon DOC percent removal and removal rate, particularly for higher $pH_0$ values. In this case, the irradiated system enabled to increase DOC percent removals and removal rates in the ranges 29 to 97%, and 19 to 65%, respectively, compared with the dark ozonation process. This is due to the high molar absorption coefficient of ozone in aqueous solution (molar absorption coefficient of 3300 L $mol^{-1}$ $cm^{-1}$ at 253.7 nm); under irradiation, $O_3$ decomposes with a quantum yield of 0.61 mol $Einstein^{-1}$ (10) and generates hydroxyl radicals from the photolysis of the hydrogen peroxide formed by the reaction of singlet oxygen atoms and water (10); it should be pointed out that the molar absorption coefficient of $H_2O_2$ is much lower (19.6 L $mol^{-1}$ $cm^{-1}$ at 253.7 nm) (10). In the case of $O_3$ and $O_3$-UV processes initiated with $pH_0$ 11, however, a fast, strong drop in pH (Figs. 3 and 4) could have favored the transition from the low selective, radical-based oxidation, to the high selective molecular attack, delaying DOC removal for longer reaction times. In experiment P7A, for example, the pH attained a minimum of 4.4 in 60 minutes, and then increased to about 8 after 120 minutes. The corresponding fast DOC removal is due to the rapid degradation of phenol and its oxidation products, generating organic acids and then achieving almost complete mineralization. A similar behavior was observed for the irradiated experiments carried out at central point conditions (LPC1 and LPC2). For the high $DOC_0$ level, a slower but important drop in pH was also observed for experiments P6 ($O_3$) and P8 ($O_3$-UV). These experimental results suggest that it is difficult to elucidate the effect of pH under reacting conditions. In fact, the mechanism of phenol ozonation consists of a complex pathway of substitution and cycloaddition reactions and, according to Beltrán (8), the ratio of concentration of dissociated and nondissociated forms of phenol varies with pH and with the reactivity with ozone. At low pH value phenol is present only in its nondissociated form while at a pH higher than the pK only the dissociated form is present. The −O- is a stronger activating group than the −OH group and, thus, the reactivity of phenol with ozone is expected to increase with the pH in such a way that the rate constants of the phenol-ozone reactions at alkaline pH are very high. Therefore, due to the complexity of the reacting system, in the experiments with the $O_3$-$H_2O_2$ process, pH was kept constant over the reaction time, in order to

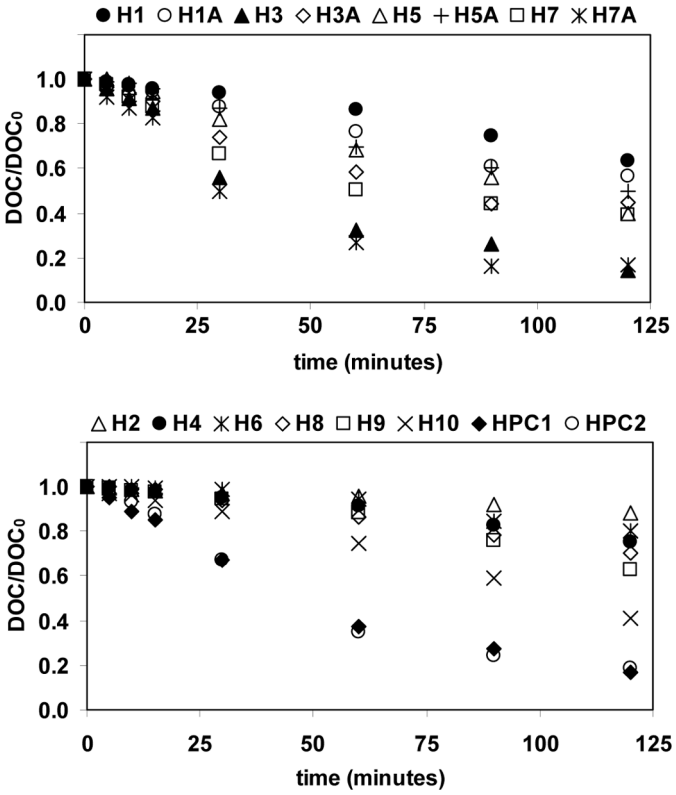


FIG. 5. Time variation of $DOC/DOC_0$ for the $O_3$-$H_2O_2$ process.

better ascertain its effect in conjunction with the effects of other variables.

For the low $DOC_0$ level, the increase in $[H_2O_2]_0$ in the $O_3$-$H_2O_2$ process favored the responses, particularly for the high ozone concentration level. In that case, an increase in the DOC percent removal in the range 18 to 54%, and an almost three-fold increase in the removal rate were obtained. The results of experiments HPC1 and HPC2 suggest that $[H_2O_2]_0$ could be lowered, in order to reduce potential scavenging effects which could have been operative at the high peroxide concentration level. In fact, depending on its concentration, $H_2O_2$ can act either as a promoter, as an indirect inhibitor of $O_3$ decomposition, or also as a radical scavenger (8). It is also worth noticing that the increase in pH from 4 to 8 favored DOC removal at the lower $[O_3]$ level, especially the removal rate, suggesting the indirect reaction mechanism associated with the dissociated form of $H_2O_2$ ($HO_2^-$). In fact, and according to Gottschalk et al. (9), this species reacts with ozone in aqueous solution with second-order reaction rates ($k = 2.2 \times 10^6\,L\,mol^{-1}\,s^{-1}$). The comparison with the reaction between ozone and $OH^-$ ($k = 70\,L\,mol^{-1}\,s^{-1}$) shows that in the $O_3$-$H_2O_2$ system the initiation step by $OH^-$ is of minor importance. Also, the reaction of $H_2O_2$ and $O_3$ is slow ($k < 10^{-2}\,L\,mol^{-1}\,s^{-1}$), as pointed out by those authors.

Summarizing to this point, the experimental results obtained in the present work show that concerning the DOC removal rate, the $O_3$-$H_2O_2$ process performed better than the $O_3$ and $O_3$-UV processes for all conditions studied. On the other hand, in terms of DOC percent removal the $O_3$-UV process provided better results in most cases. Finally, for the high $DOC_0$ level, the $O_3$-$H_2O_2$ system performed better than the $O_3$ and $O_3$-UV processes concerning the analyzed responses.

## Neural Networks Modeling

In this work, modeling phenol degradation by the $O_3$, $O_3$-UV, and $O_3$-$H_2O_2$ processes accounted for the following:

i. in the present study, only DOC concentration was monitored over time, although a large variety of degradation products have been identified (2);
ii. the reactivity of ozone with organic dissociating compounds strongly depends on pH. Reactions with ozone are pH dependent, so that the increase in ozonation rate with pH can be due not only to indirect reactions but also to direct reactions (8,9);
iii. oxidation of phenol by ozone and radical species follows complex chain steps;
iv. the reacting system depends on mass transfer phenomena (associated with the specific kinetic regime of ozone absorption (8),) as well as on the radiation field (in the $O_3$-UV process). Mass transfer depends on the pH, composition, gas flow rate, ozone concentration in the gas phase, bubble size, etc. As a result, the phenomenological modeling of the $O_3$, $O_3$-UV, and $O_3$-$H_2O_2$ processes is a difficult task.

The development of detailed models is also complicated by the fact that a large amount of organic oxidation products can be formed, many of which are unknown. Such compounds can act as scavengers or initiators, and take part in many side reactions as well, for which rate constants are required (9). Moreover, in real wastewaters the organic-inorganic matrix is too complex and individual concentrations of species cannot be used to study the kinetics of ozone-based processes (8). Kinetic modeling based on lumped parameters (e.g., DOC) has been used to surmount these difficulties and describe the behavior of experimental DOC-time data such as those of Figs. 3–5. Lumped kinetic models consider few reactions to represent all possible direct and indirect reactions of ozone with organic compounds present in water (referred to DOC as a lumped parameter, for example), and the reaction between hydroxyl radicals generated from the ozone decomposition and the DOC (8). Although it is questionable whether it is possible to lump all reactions in complex aqueous matrices together (9), the literature presents many examples in which lumped kinetic models suitably

described the oxidation of pollutants by ozone (11–14). As an alternative approach, based on these peculiarities and on previous studies published by the authors (e.g., 15,16), empirical models based on artificial neural networks (NN) are used in this work. Fundamental aspects of NN are presented elsewhere (17). They are able to extract information from experimental data and to deal with the non-linearity and inherent complexity of a given process in an efficient manner, and have been applied to ozone reacting systems (18,19).

In this work, three-layer feed-forward NN models with activation functions of the sigmoid type (20) were used to fit experimental data. For the $O_3$ and $O_3$-UV processes, the following input variables were considered: the initial dissolved organic carbon concentration, $DOC_0$; ozone concentration in the gas phase, $[O_3]$; pH at time $t$; presence or absence of UVC radiation; time. The output variable was the DOC at a given time ($DOC_t$). For the $O_3$-$H_2O_2$ process, the initial hydrogen peroxide concentration, $[H_2O_2]_0$, replaced UVC radiation, with all other variables kept the same. All variables were normalized in the range 0.1–0.9.

Fitting of the NN models was based on the back propagation algorithm, with a total of 10,000 presentations of the data set to the NN. The fitting procedure consisted of minimizing the sum of quadratic deviations $E$ between calculated and experimental values of the output variable (16) by varying the number of neurons in the hidden layer (NH). In any case, previous data analysis enabled to detect outliers on the basis of experimental evidence. This was accomplished by a technique described by Alves and Nascimento (21) that consists of a preliminary NN fitting using the entire data set, in order to obtain a reasonable result with a minimum NH value and a low number of iterations. After elimination of outliers from the experimental data, the remaining data pairs were randomly distributed into the learning (LS) and test (TS) sets, in such a way that about 35% of the data were used in validation. The lowest number of neurons in the hidden layer was the heuristic rule approach for model evaluation. A simple measure of the quality of fitting of a given NN is given by:

i. the variation of the quadratic deviations based on the data of the learning and test sets ([E(LS)] and



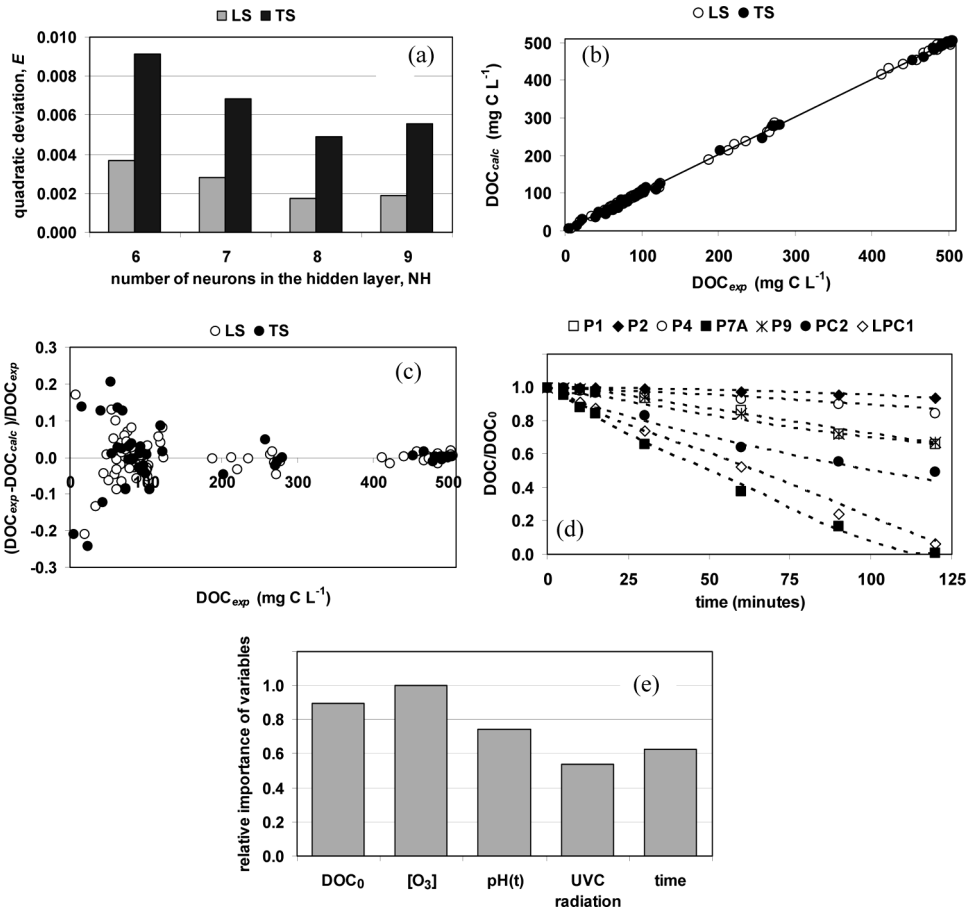


FIG. 6. Neural network results for the $O_3$ and $O_3$-UV processes. In 5d, symbols and dotted lines refer to experimental and simulated values, respectively.

[E(TS)], respectively) with the number of neurons in the hidden layer;

ii. the scatter of the data points around the 45° line in a graph that compares the values calculated by the NN versus the experimental data, measured by the angular coefficient ($\alpha$) and the determination coefficient ($R^2$) of this line;

iii. the distribution of relative deviations $(DOC_{exp} - DOC_{calc})/DOC_{exp}$ between experimental ($DOC_{exp}$) and calculated ($DOC_{calc}$) values; and

iv. a graphical comparison of calculated and experimental DOC-time values.

For the $O_3$ and $O_3$-UV processes, a NN with NH = 8 corresponded to the best configuration (Fig. 6a). The agreement between model predictions and the experimental data is good for both data sets (Fig. 6b), with $\alpha = 1$ and $R^2 = 0.999$ for both the LS and TS. The data of the TS are well distributed in the whole experimental domain. The values of $(DOC_{exp} - DOC_{calc})/DOC_{exp}$ are reasonably well distributed in the domain of experimental data, and they decrease for higher DOC values (Fig. 6c). Most deviations lie in the range ±10%, with maximum values of 21.1% and 24.3% for the LS and TS, respectively; nevertheless, these values represent less than 6 mg C $L^{-1}$. Figure 6d compares calculated and experimental values of the output variable for selected experiments, and confirms the very good quality of fitting. While the information fed to a NN model is distributed over its neurons, the relative importance of the input variables can be evaluated by comparing the weights associated with each input variable to the NN model and the first NN layer (16). For NH = 8, 57 weights were calculated: 48 between the input and hidden layers (5 weights plus a bias term for each neuron in the hidden layer), and 9 between the hidden and output layers (8 weights plus a bias term); the sums of the absolute values of the weights are plotted in Fig. 6e. Ozone concentration, $DOC_0$, and pH showed the largest effects upon the DOC-time behavior.

In the case of the $O_3$-$H_2O_2$ processes, a NN with NH = 9 provided the best configuration (Fig. 7a). The values of $\alpha$ and $R^2$ were 0.995 and 0.998 for the LS, respectively and 0.990 and 0.998 for the TS, respectively. Again, most values of the relative deviations $(DOC_{exp} - DOC_{calc})/DOC_{exp}$ lie in the range ±10%; however, maximum differences close to 30% and 25% were obtained for the LS and TS,



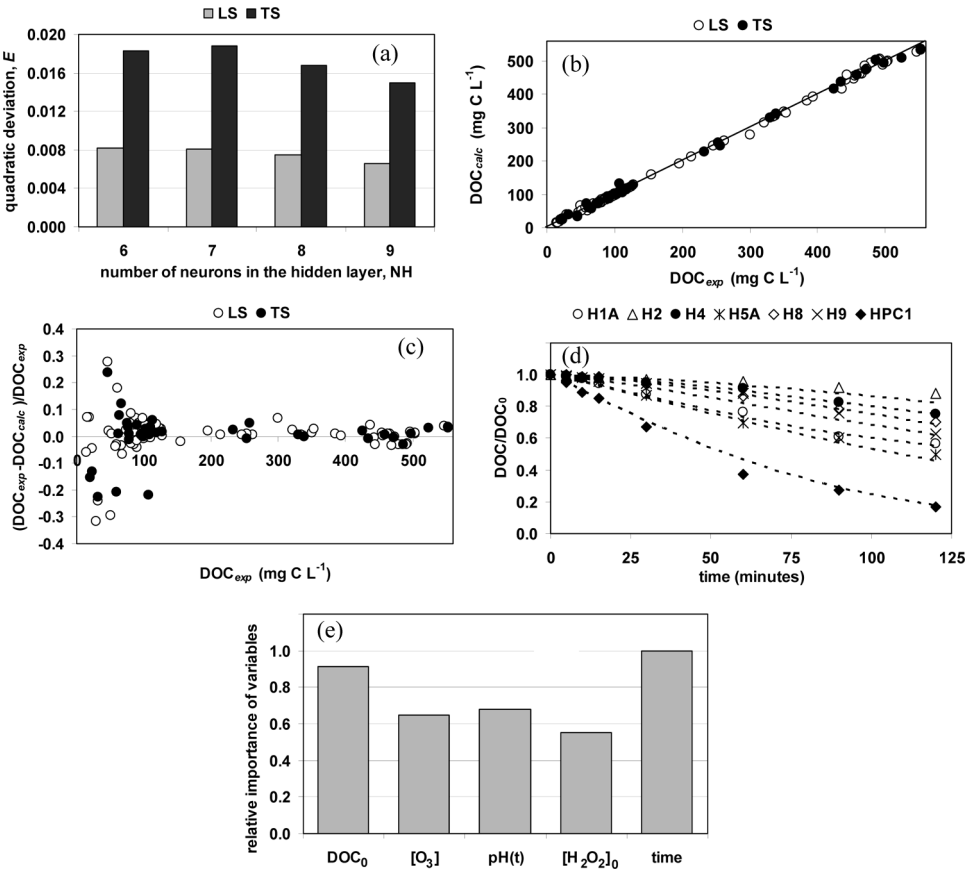


FIG. 7. Neural network results for the $O_3$-$H_2O_2$ process. In 6d, symbols and dotted lines refer to experimental and simulated values, respectively.

respectively, which correspond to about $10\,mg\,C\,L^{-1}$ (LS) and $23.7\,mg\,C\,L^{-1}$ (TS). These results confirm the good agreement between model predictions and experimental data (Figs. 7b–d). Figure 7e shows that ozone concentration, pH, and $[H_2O_2]_0$ had similar effects upon the DOC-time evolution, while a large effect of $DOC_0$ was again observed.

## CONCLUSION

In most cases, for low initial DOC, the $O_3$-$H_2O_2$ process performed better than the $O_3$ and $O_3$-UV systems in terms of DOC removal rate for both hydrogen peroxide concentration levels. For DOC removed in 120 minutes; however, a strong dependence on ozone and $H_2O_2$ concentrations was verified. The developed artificial neural networks models adequately fitted the experimental results and can be conveniently used to predict the DOC-time evolution and DOC removal rates. These models can be coupled with mass balances to simulate the processes for different values of the input variables.



## ACKNOWLEDGEMENTS

The authors wish to thank the support by FAPESP (Fundação de Amparo à Pesquisa do Estado de São Paulo), CAPES (Coordenação de Aperfeiçoamento de Pessoal de Nível Superior), and CNPq (Conselho Nacional de Desenvolvimento Científico e Tecnológico).

## REFERENCES

1. Kusic, H.; Koprivanac, N.; Bozic, A.L. (2006) Minimization of organic pollutant content in aqueous solution by means of AOPs: UV- and ozone-based technologies. *Chem. Eng. J.*, 123 (3): 127–137.
2. Beltrán, F.J.; Rivas, F.J.; Gimeno, O. (2005) Comparison between photocatalytic ozonation and other oxidation processes for the removal of phenols from water. *J. Chem. Technol. Biotechnol.*, 80 (9): 973–984.
3. Esplugas, S.; Gimenez, J.; Contreras, S.; Pascual, E.; Rodriguez, M. (2002) Comparison of different advanced oxidation processes for phenol degradation. *Water Res.*, 36 (4): 1034–1042.
4. Poznyak, T.; Vivero, J. (2005) Degradation of aqueous phenol and chlorinated phenols by ozone. *Ozone Sci. Eng.*, 27 (6): 447–458.
5. Mvula, E.; von Sonntag, C. (2003) Ozonolysis of phenols in aqueous solution. *Org. Biomol. Chem.*, 1 (10): 1749–1756.
6. Mokrini, A.; Ousse, D.; Esplugas, E. (1997) Oxidation of aromatic compounds with UV radiation/ozone/hydrogen peroxide. *Water Sci. Technol.*, 35 (4): 95–102.
7. Huang, C.R.; Shu, H.Y. (1995) The reaction-kinetics, decomposition pathways and intermediate formations of phenol in ozonation, UV/$O_3$ and UV/$H_2O_2$ processes. *J. Hazard. Mater.*, 41 (1): 47–64.
8. Beltrán, F.J. (2004) *Ozone Reaction Kinetics for Water and Wastewater Systems*, 1st Ed.; Lewis Publishers: Boca Raton, FL.
9. Gottschalk, C.; Libra, J.A.; Saupe, A. (2000) *Ozonation of Water and Waste Water*, 1st Ed.; Wiley-VCH: Weinheim, Germany.
10. Oppenländer, T. (2003) *Photochemical Purification of Water and Air*, 1st Ed.; Wiley-VCH: Weinheim, Germany.
11. Beltrán, F.J.; Encinar, J.M.; García-Araya, J.F. (1995) Modelling industrial wastewater ozonation in bubble contactors. 2. Scale-up from bench to pilot plant. *Ozone Sci. Eng.*, 17 (4): 379–398.
12. Andreozzi, R.; Caprio, V.; Insola, A.; Tufano, V. (1996) Measuring ozonation rate constants in gas-liquid reactors under the kinetic-diffusional transition regime. *Chem. Eng. Commun.*, 143: 195–204.
13. Azevedo, E.B.; Neto, F.R.D.; Dezotti, M. (2006) Lumped kinetics and acute toxicity of intermediates in the ozonation of phenol in saline media. *J. Hazard. Mater.*, 128 (2–3): 182–191.
14. Santos, A.; Yustos, P.; Rodriguez, S.; Vicente, F.; Romero, A. (2008) Detoxification kinetic modeling for nonbiodegradable wastewaters: An ecotoxicity lumping approach. *Ind. Eng. Chem. Res.*, 47 (22): 8639–8644.
15. Teixeira, A.C.S.C.; Guardani, R.; Nascimento, C.A.O. (2003) Solar photochemical degradation of aminosilicones contained in liquid effluents. Process studies and neural network modeling. *Ind. Eng. Chem. Res.*, 42 (23): 5751–5761.
16. Nogueira, K.R.B.; Teixeira, A.C.S.C.; Nascimento, C.A.O.; Guardani, R. (2008) Use of solar energy in the treatment of water contaminated with phenol by photochemical processes. *Braz. J. Chem. Eng.*, 25 (4): 671–682.
17. Zupan, J.; Gasteiger, J. (1999) *Neural Networks in Chemistry and Drug Design*, 2nd Ed.; Wiley-VCH: Weinheim, Germany.
18. Oguz, E.; Tortum, A.; Keskinler, B. (2008) Determination of the apparent rate constants of the degradation of humic substances by ozonation and modeling of the removal of humic substances from the aqueous solutions with neural network. *J. Hazard. Mater.*, 157 (2–3): 455–463.
19. Poznyak, T.; Chairez, I.; Poznyak, A. (2005) Application of a neural observer to phenols ozonation in water: Simulation and kinetic parameters identification. *Water Res.*, 39 (12): 2611–2620.
20. Göb, S.; Oliveros, E.; Bossmann, S.H.; Braun, A.M.; Nascimento, C.A.O.; Guardani, R. (2001) Optimal experimental design and artificial neural networks applied to the photochemically enhanced Fenton reaction. *Water Sci. Technol.*, 44 (5): 339–345.
21. Alves, R.M.B.; Nascimento, C.A.O. (2002) Gross errors detection of industrial data by neural network and cluster techniques. *Braz. J. Chem. Eng.*, 19 (4): 483–489.